JOURNAL OF MATERIALS SCIENCE 27 (1992) 5315–5319

Some performance characteristics of a solid-state battery composed of Chevrel phase, a copper-ion conductor, and Prussian blue

K. KUWABARA, J. ITOH, K. SUGIYAMA
Department of Applied Chemistry, Faculty of Engineering, Nagoya University, Chikusa-ku, Nagoya 464-01, Japan

A solid-state battery composed of copper molybdenum sulphide (Chevrel phase: CP), copper-ion conductive solid electrolyte, and iron hexacyanoferrate complex (Prussian blue: PB), was studied from the viewpoint of its applicability to a recyclable energy source. The electromotive force increased with the copper content of the CP. The discharge capacity increased with increasing sulphur content as well as copper content of the CP. The discharge–charge cycling behaviour indicated that both CP and PB containing a three-dimensional open structure were potential electrode materials for a promising rechargeable battery.

1. Introduction

Secondary solid-state batteries using solid electrodes and solid electrolyte are of great interest in the field of power sources for microelectronic devices because of their advantages of long self life and no leakage of electrolyte. For the electrode materials, high ionic and electronic mixed conduction is required to guarantee the smooth electrochemical reactions.

Ternary molybdenum sulphides $M_xMo_6S_{8-y}$ (M denotes a metal), called Chevrel-phase compounds, are candidates for electrode materials [1–3]. The crystal structure of the Chevrel phase with smaller M atoms such as copper is composed of Mo_6S_{8-y} groups stacked in three dimensions and of metal atoms located near the body-centred positions surrounded by the Mo_6S_{8-y} groups [4]. Metal atoms are expected to migrate easily along the three-dimensional pathway network formed in the structure. At room temperature, the Chevrel phase shows moderate electronic conduction based on the hopping of molybdenum d electrons. Thus, the Chevrel phase is an ionic–electronic mixed conductor [5].

A hexacyano-iron polynuclear complex, Prussian blue (PB), is also a mixed conductor [6]. The crystal structure of the soluble PB containing potassium ions consists of alternating iron (II) and iron (III) located on a face-centred cubic lattice where the iron (III) and iron (II) ions are surrounded octahedrally by nitrogen and carbon atoms, respectively [7]. Such a structure contains a three-dimensional open channel through which some ions intercalate and migrate. Furthermore, the mixed valence transition-metal hexacyanides reversibly change the oxidation and reduction states without changing the crystal structure [8]. The electronic conduction in an electric field is based on the hopping mechanism.

The copper Chevrel phase (CP) was used both as the anode and cathode of a battery [1, 3], which can be classified into a kind of copper concentration cell. Secondary batteries with the PB were reported by Neff [9] and Kaneko [10, 11]. According to these authors, both the anode and the cathode consisted of PB membranes electrochemically deposited on a substrate. Such batteries can also be regarded as a sort of concentration cell.

No work on a battery using CP as the anode and PB as the cathode has been reported. Recently, we have found that PB powder is useful as a cathode-active material for a secondary solid-state cell [12]. This paper describes the performance characteristics of a solid-state battery composed of CP, a solid electrolyte, and the soluble PB powder.

2. Experimental procedure

2.1. Materials

The copper-ion conductor, $Rb_4Cu_{16}I_{6.75}Cu_{13.25}$, was prepared by the same procedure as reported in an earlier paper [13]. Appropriate amounts of RbCl, CuI, and CuCl were mixed in an agate ball mill. Tablets of the mixture were heated at 200 °C for 17 h in an evacuated Pyrex tube, and then were annealed at 130 °C for 17 h.

The CP, $Cu_xMo_6S_{8-y}$, was prepared by direct reaction of powders of copper, molybdenum, and sulphur. After the powders were mixed in an agate mortar and pestle, tablets of the mixture were formed, and sealed in a quartz tube under vacuum. The specimens were heated at 400 °C for 18 h, at 600 °C for 18 h, and then at 1000 °C for 24 h. Referring to the formation diagram of the CP at 1000 °C [14], the samples were prepared within the single-phase region between

0022–2461

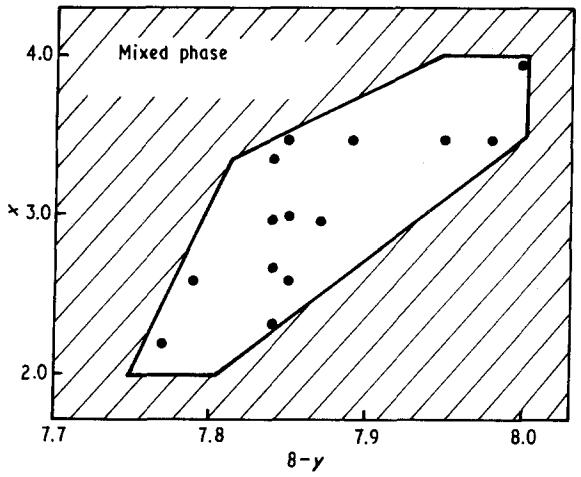

Figure 1 Single-phase region (enclosed area) of the Chevrel phase $Cu_xMo_6S_{8-y}$. (●) Composition investigated in this study.

$2.0 \leqslant x \leqslant 4.0$ and $7.75 \leqslant (8 - y) \leqslant 8.00$, as shown in Fig. 1. All the samples were examined by powder X-ray diffraction technique.

The PB powder sample, $KFe[Fe(CN)_6]$, was a first grade chemical and was used without further purification.

2.2. Battery performance

The solid-state batteries examined were button-type galvanic ones. The anode was a mixture of the CP and the solid electrolyte. Because the mixture composition of the anode influenced considerably the performance characteristics of the battery, on the basis of pre-experimental data, the weight ratio of electrolyte to CP leading to the best result was determined to be 2.0. The cathode consisted of PB (0.2 g), electrolyte (0.4 g), and graphite powder (0.06 g). These appropriate amounts were obtained in the previous study [12]. The anode, electrolyte, and cathode layers were pressed simultaneously at 300 MPa to form a single cell of 13 mm diameter and 3 mm thick.

The electromotive force (e.m.f.) of each battery was measured 24 h after cell formation. The discharge behaviour was examined at a constant current of 50–500 μA/cell (38–382 μA cm^{-2}). The discharge–charge performance was investigated at 50 μA/cell. The cycling was carried out in both ways with and without a rest time. All the measurement temperatures were maintained at 25 °C using a thermostat.

3. Results and discussion

3.1. E.m.f. of the battery

The e.m.f. of the battery treated in this study depended on the anode composition, namely on the composition of CP, because the cathode composition was kept constant. Fig. 2 shows an example of the e.m.f. values of the batteries with CP of various sulphur content $(8 - y)$ at a fixed copper composition. A slight decreasing tendency was observed with increasing sulphur content, whereas the e.m.f. value clearly increased with increasing copper content of the CP at a fixed sulphur composition, as shown in Fig. 3.

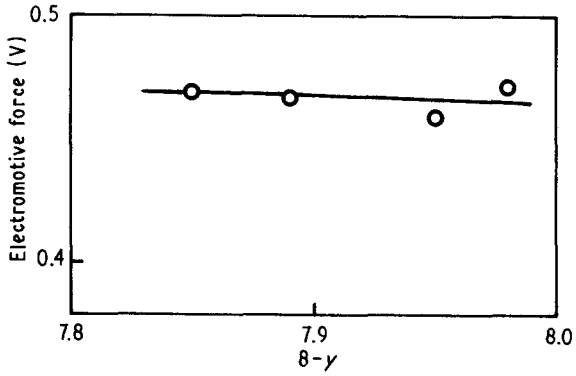

Figure 2 The e.m.f. of the CP/PB battery. The CP composition is $Cu_{3.48}Mo_6S_{8-y}$.

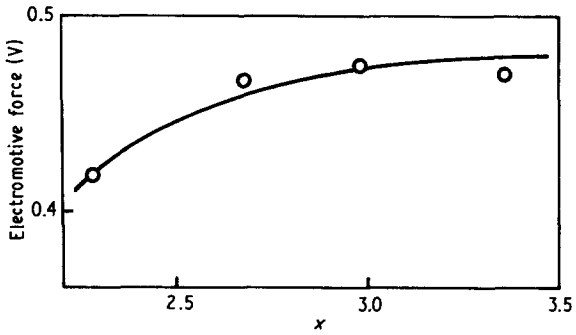

Figure 3 The e.m.f. of the battery with the CP of $Cu_xMo_6S_{7.84}$.

The e.m.f. of the galvanic cell is based on the electrochemical reactions both in the anode and in the cathode. The CP anode is oxidized to supply copper ions towards the cathode through the electrolyte, and the PB cathode is reduced to receive copper ions. In principle, when the copper concentration in the CP is higher, a higher e.m.f. value must be given. In Fig. 3, the e.m.f. value in the lower x region followed the principle, while the increasing rate of the e.m.f. slowed down with the increasing x. This fact suggests that the rate of increase of copper activity in the CP decreased with increasing x. The e.m.f. in Fig. 2 was surmised to be independent of the sulphur composition. However, because the increase in sulphur content results in a relative decrease of copper content of the CP, the slight e.m.f. change may also be said to follow the above principle.

3.2. Discharge capacity

The constant current discharge curves are shown in Fig. 4 as an example at a fixed copper composition ($x = 3.48$) in the CP. Depending on the sulphur composition, a variety of discharge behaviour was observed.

In order to determine the appropriate composition of the CP, the discharge capacity was estimated tentatively using the current and the duration up to the time when the cell voltage fell to 50% of the e.m.f. value. Figs 5 and 6 show the discharge capacities defined

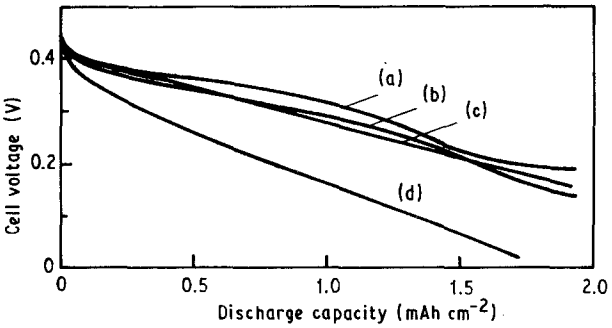

Figure 4 Constant current discharge curves for the CP/PB battery. The sulphur content $(8 - y)$ of $Cu_{3.48}Mo_6S_{8-y}$ is (a) 7.95, (b) 7.89, (c) 7.98 and (d) 7.85.

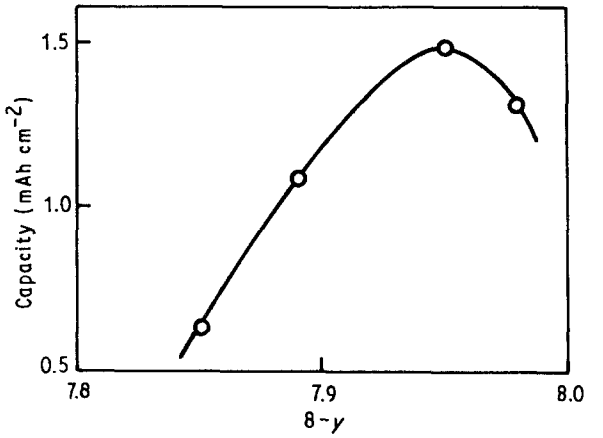

Figure 5 Discharge capacity of the CP/PB battery. The CP composition is $Cu_{3.48}Mo_6S_{8-y}$.

above, plotted against the sulphur and copper composition in the CP, respectively. Fig. 5 indicates the steep increase of the discharge capacity with increasing $(8 - y)$ up to 7.95. The slight drop at 7.98 seems to come from any contamination of the CP, because the specimen of $(8 - y) = 7.98$ existed near the single-phase/mixed-phase boundary [14]. A moderate increase of the discharge capacity is observed in Fig. 6 with increasing x.

The change in the discharge capacity with composition change of the CP is supposed to relate to the mobility as well as the concentration of copper atoms in the anode, because the voltage loss in the anode will be reduced if the mobility or the conductivity of the copper atom is high at a constant concentration of copper atoms. The atomic mobility depends on the width of the pathway in the CP lattice. If a certain pathway of sufficient width in the crystal lattice is made ready for atomic migration, the CP with a higher concentration of copper atoms must be able to supply more copper ions migrating towards the cathode, which leads to an increase of the discharge capacity.

The dependence of lattice parameters on the composition was discussed by Yamamoto *et al.* [14]. The lattice parameters of the rhombohedral unit cell of $Cu_xMo_6S_{8-y}$ are represented by the edge length a and the angle α. According to the authors, both a and α decreased slightly with increasing sulphur content

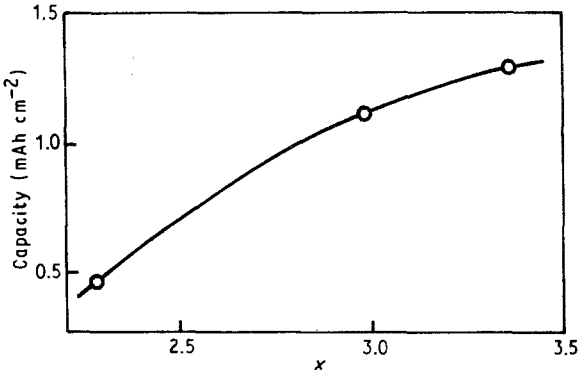

Figure 6 Discharge capacity of battery with the CP of $Cu_xMo_6S_{7.84}$.

$(8 - y)$ at a certain constant copper content. When the copper content was varied at a constant sulphur composition, both a and α increased linearly with increasing x. The increase of the discharge capacity shown in Fig. 5 suggests that the small decrease in the lattice parameters with increasing $(8 - y)$ was caused by a slight contraction of the Mo_6S_{8-y} group, which resulted in a favourable expansion of the tunnel for copper-atom migration. On the other hand, the increasing rate of discharge capacity shown in Fig. 6 was not as high as expected from the increase of copper-atom concentration. This seems to be caused by the voltage loss due to the decrease of copper-atom mobility with increasing x. The enlargement of the lattice parameters with increasing x was based on the coulombic repulsion between copper atoms and copper and molybdenum atoms. The coulombic repulsion may have resulted in a hindering effect for copper-atom migration.

3.3. Discharge performance

The results for the discharge capacities indicated that both the copper and sulphur contents of the CP were required to be higher in order to obtain good performance of the battery. Thus, the CP composition $Cu_{3.48}Mo_6S_{7.95}$ was employed in the following experiments.

Fig. 7 shows the cell voltage versus time curves at several constant currents. The cell voltages fell with the depth of discharge, and several curves were S-shaped in two steps. As reported in a previous paper [12], the S-shaped curves suggest that a one-phase reaction corresponding to each step proceeded in the cathode of the battery [15]. The two-steps in the curves appear to be caused by any change in the CP, because such a two-step curve was absent in a Cu/PB cell. According to structure analysis with X-ray diffraction [4], the CP has two sets of six equivalent copper sites per unit cell. Kanno *et al.* [1] studied coulometric titration using a solid-state electrochemical cell and observed distinct potential changes due to the difference in energy levels of the two sets of sites.

From the discharge curve, the capacity was estimated using the current and time. The cut-off voltage was determined to be half the e.m.f. value (0.48 V). The

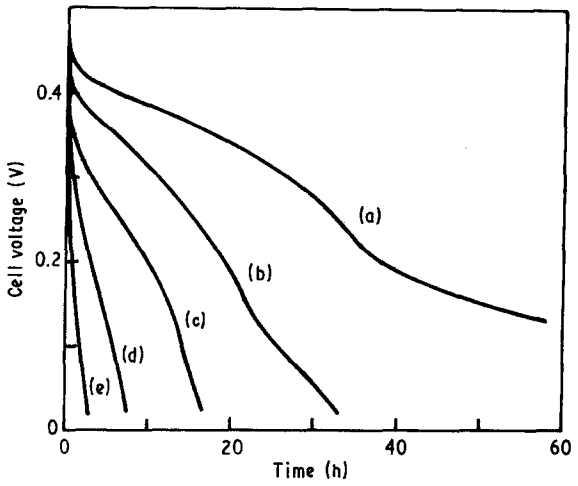

Figure 7 The discharge performance of the battery at a constant current of (a) 50, (b) 100, (c) 200, (d) 300 and (e) 500 μA/cell.

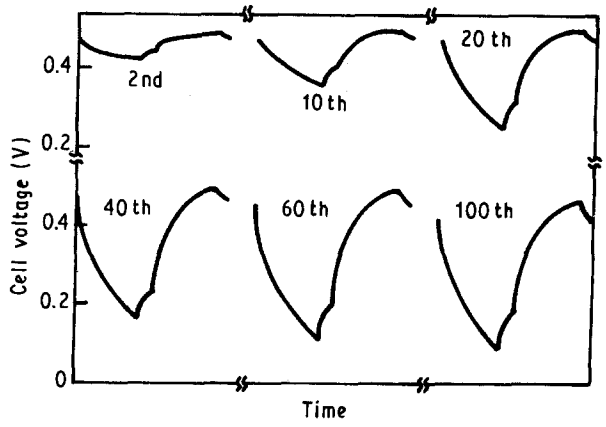

Figure 8 The discharge (50 min)–charge (50 min) performance of the CP/PB battery with rest time (10 min). The current is 50 μA/cell.

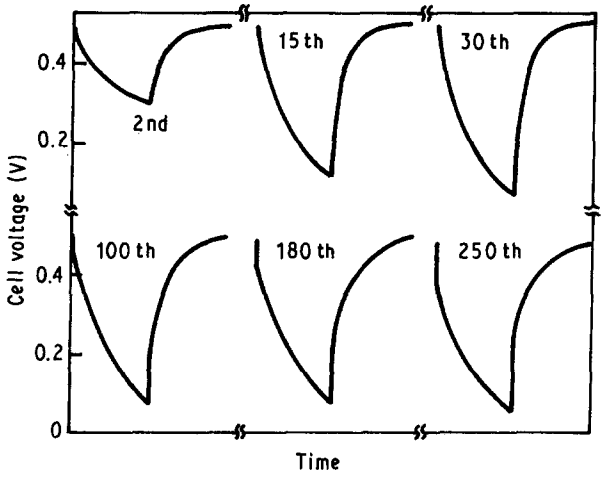

Figure 9 The discharge (30 min)–charge (30 min) curves of the battery without rest time at 50 μA/cell.

capacity values were not always higher than those expected and decreased from about 1.9 mAh at 50 μA/cell to about 0.3 mAh at 500 μA/cell. The theoretical anode capacity was calculated, supposing an anode reaction

$$Cu_{3.48}Mo_6S_{8-y} \rightarrow 3.48Cu^+ + Mo_6S_{8-y} + 3.48e^- \quad (1)$$

to be 17.7 mAh. Therefore, the anode efficiency ranged from 11%–1.5%, corresponding to the increase in the discharge current. As a result of the discharge, the copper content of the CP changed from the initial value $x = 3.48$ to $x = 3.10$–3.43 at the cut-off point. On the other hand, the calculated cathode capacity referring to a cathode reaction

$$Cu^+ + KFe[Fe(CN)_6] + e^- \rightarrow CuKFe[Fe(CN)_6] \quad (2)$$

was 17.5 mAh. Thus, the cathode efficiency was estimated to range from 11%–1.5%. The anode and cathode efficiencies mentioned above were fairly low. Considering the high mobility of copper atoms in the CP and the PB lattices, it seems that in addition to bulk resistance of each component, the CP/electrolyte or the electrolyte/PB interface resistance suppressed the discharge capacity or the efficiencies.

3.4. Discharge–charge performance

The discharge–charge performance was examined to determine the recyclability of the CP/PB battery. The representative cycling curves with rest time are shown in Fig. 8. At the beginning of cycles the cell voltage decreased gradually with cycling. However, the voltage drop subsided little by little around the 40th cycle, and the discharge–charge curve displayed almost the settled form from the 60th cycle to the 500th or more cycle. In the cycling test of the Cu/PB battery without rest time [12], the abrupt voltage changes, such as *iR* drop, were observed at the starting points of the discharge–charge operation, whereas such abrupt changes of voltage are absent in the cycling curves shown in Fig. 8. This seems to be caused by setting the rest time. The copper ions may not be accumulated at the surface of the electrode-active materials, but may diffuse from the surface to the bulk of the PB or the CP during the rest time. The ions diffusing in the bulk are supposed to migrate smoothly in the reverse direction at the next charge–discharge operation, which may have suppressed the appreciable *iR* drops.

Fig. 9 indicates another representative behaviour of cycling without rest time. In this case, the form of the discharge–charge curve settled at about the 30th cycle, and the stable cycling continued more than 500 times. The anode and cathode mixtures used for the battery had resistances of about 140 and 320 Ω respectively, which were measured by a d.c. two-terminal method. From the resistances of the electrode and electrolyte layers, the total *iR* drop at 50 μA/cell was estimated to be about 30 mV. The sudden voltage changes in the steady state cycling region in Fig. 9 were larger than 30 mV. This appears to be caused by the CP/electrolyte or electrolyte/PB interface resistance, which must be reduced in future work.

4. Conclusion

Performance characteristics of a solid-state battery,

(CP, X)|X|(PB, X, C) (X denotes a copper-ion conductor), were examined, and the following new results were obtained.

1. The e.m.f. increased with increasing copper content in the CP within the single phase.

2. The discharge capacity increased for the most part with increasing sulphur and copper contents.

3. The cell voltage in the discharge–charge operation reached a steady state after several tens of cycles, and the stable cycling performance was maintained for more than 500 times.

These results proved that both CP and PB were excellent electrode materials. In addition, the experimental facts revealed that the solid-state CP/PB cell was a new promising candidate for a rechargeable battery.

References

1. R. KANNO, Y. TAKEDA, M. OHYA and O. YAMAMOTO, *Mater. Res. Bull.* **22** (1987) 1283.
2. T. UCHIDA, Y. TANJO, M. WAKIHARA and M. TANIGUCHI, *J. Electrochem. Soc.* **137** (1990) 7.
3. T. SOTOMURA, S. ITOH, S. KONDO and T. IWAI, *Denki Kagaku* **59** (1991) 129.
4. K. YVON, A. PAOLI, R. FLÜKIGER and R. CHEVREL, *Acta Crystallogr.* **B33** (1977) 3066.
5. G. J. DUDLEY, K. Y. CHEUNG and B. C. H. STEELE, *J. Solid State Chem.* **32** (1980) 259.
6. D. ELLIS, M. ECKHOFF and V. D. NEFF, *J. Phys. Chem.* **85** (1981) 1225.
7. J. F. KEGGIN and F. D. MILES, *Nature* **137** (1936) 577.
8. K. ITAYA, I. UCHIDA and V. D. NEFF, *Acc. Chem. Rev.* **19** (1986) 162.
9. V. D. NEFF, *J. Electrochem. Soc.* **132** (1985) 1382.
10. M. KANEKO, *J. Polym. Sci. C Polym. Lett.* **24** (1986) 435.
11. M. KANEKO and T. OKADA, *J. Electroanal. Chem.* **255** (1988) 45.
12. K. KUWABARA, J. NUNOME and K. SUGIYAMA, *J. Electrochem. Soc.* **137** (1990) 2001.
13. T. TAKAHASHI, R. KANNO, Y. TAKEDA and O. YAMAMOTO, *Solid State Ionics* **3,4** (1981) 283.
14. S. YAMAMOTO, K. MATSUI, M. WAKIHARA and M. TANIGUCHI, *Mater. Res. Bull.* **18** (1983) 1311.
15. A. KOZAWA and R. A. POWERS, *J. Electrochem. Soc.* **113** (1966) 870.

Received 13 June
and accepted 31 October 1991